Time-dependent isospin composition of particles emitted in fission events following ^{40}Ar + ^{197}Au at 35 MeV/u

R. S. Wang (王仁生),[1] Y. Zhang (张嫣),[1] Z. G. Xiao (肖志刚),[1,2,*] J. L. Tian (田俊龙),[3] Y. X. Zhang (张英逊),[4] Q. H. Wu (吴强华),[4] L. M. Duan (段利敏),[5] G. M. Jin (靳根明),[5] R. J. Hu (胡荣江),[5] S. F. Wang (王素芳),[5] Z. Y. Li (李祖玉),[5] H. W. Wang (王宏伟),[6] Z. Zhang (张钊),[1] H. Yi (易晗),[1] H. J. Li (李红洁),[1] W. J. Cheng (程文静),[1] Y. Huang (黄彦),[1] and L. M. Lü (吕黎明)[1]

[1]*Department of Physics, Tsinghua University, Beijing 100084, China*

[2]*Collaborative Innovation Center of Quantum Matter, Beijing 100084, China*

[3]*School of Physics and Electrical Engineering, Anyang Normal University, Anyang 455000, China*

[4]*China Institute of Atomic Energy, Beijing 102413, China*

[5]*Institute of Modern Physics, Chinese Academy of Sciences, Lanzhou 730000, China*

[6]*Shanghai Institute of Applied Physics, Chinese Academy of Sciences, Shanghai 201800, China*

(Received 14 February 2014; revised manuscript received 24 April 2014; published 27 June 2014)

Fission fragments resulting from the fission of target-like nuclei produced in the ^{40}Ar + ^{197}Au reaction at 35 MeV/u are measured in coincidence with the emitted light charged particles (LCPs). Comparison of the N/Z composition of the LCPs at middle and large angles in the laboratory frame shows that particles emitted at smaller angles, which contain a larger contribution from dynamical emission, are more neutron rich. A moving-source model is used to fit the energy spectra of the hydrogen isotopes. A hierarchy from proton to deuteron and triton is observed in the multiplicity ratio between the intermediate velocity source and the compound nucleus source. This ratio is sensitive to the dynamical emission at early stages of the reaction and to statistical emission lasting up to the scission point. Calculations with the improved quantum molecular dynamics (ImQMD) transport-model qualitatively support the picture that more free and bound neutrons are emitted during the early stage, showing a clear dependence of N/Z on the parametrization of the symmetry energy. The time-dependent isospin composition of the emitted particles thus may be used to probe the symmetry energy at subsaturation densities.

DOI: 10.1103/PhysRevC.89.064613 PACS number(s): 25.70.Jj, 25.60.−t, 24.10.Lx

I. INTRODUCTION

One of the main purposes of heavy ion collisions over a wide beam-energy range from Fermi energies to energies of the CERN Large Hadron Collider is to study the equation of state (EOS) of strong-interaction matter. In the hadronic phase, the symmetry-energy term $E_{\rm sym}(\rho)$ in the EOS of isospin-asymmetric nuclear matter is an essential input for modeling the structure and properties of neutron stars as well as for calculating the reaction dynamics that the exotic nuclei undergo. Although some progress has been made in constraining $E_{\rm sym}(\rho)$ at subsaturation densities by using both terrestrial nuclear laboratory data and astrophysical observations [1,2], quantitative elucidation of the density dependence of $E_{\rm sym}(\rho)$ remains one of the major tasks in nuclear physics.

The importance of the isospin asymmetry-dependent potential in the formation of neutron skin as well as in the two-body heavy ion collisions at Fermi energies was discussed earlier using the Boltzmann–Uehling–Uhlenback equation [3]. Due to the symmetry energy, the neutron skin is enhanced and can further lead to a neutron-rich neck and modify the deflection function in two-body heavy-ion collisions. A density-dependent symmetry energy means that protons and neutrons experience different potentials and this drives more neutrons than protons into the gas phase during the evolution of the hot system formed in heavy-ion collisions. This phenomenon, knows as isospin fractionation [4], is regarded as direct evidence that the drift of the isospin degree of freedom varies along with the density of nuclear matter. Isospin diffusion, which describes the transport of neutrons or protons resulting from the isospin gradient between a projectile and a target with different N/Z composition, has been identified in ^{112,124}Sn + ^{112,124}Sn reactions and applied to constrain $E_{\rm sym}(\rho)$ at subsaturation densities [5–8]. Other probes such as the pre-equilibrium neutron-to-proton ratio [9,10], isoscaling [11], the neutron skin thickness of the ^{208}Pb nucleus [12], the giant monopole resonance [13], the N/Z ratio of the fragments [14], hard gamma emissions [15], small angle correlation function [16–19] and the systematics of the nuclear binding energies [20] have been used to constrain the symmetry energy at subsaturation densities. Within a certain uncertainty interval, a consistent density dependence of the symmetry energy has been obtained [2].

Although some of the probes used operate on a short time scale, it is pointed out that the observables originating from sufficiently long time process in heavy-ion collisions in the Fermi energy regime are favored since a long-lived process is more sensitive to the underlying density-dependent potential [21]. More probes originating from the process with a wide range of time scale have recently been proposed to constrain the symmetry energy. For instance, it was found by Rizzo that the cross section of heavy-ion fusion at low energy exhibited certain dependence on the symmetry energy at the saturation point [22]. Dynamic binary decay of the heavy excited projectile-like fragments (PLF*) in ^{124,136}Xe + ^{112,124}Sn

*xiaozg@tsinghua.edu.cn

at 50 MeV/u has been studied. In this work the neutron richness of the light fragment from the decay of the PLF* is correlated with the rotation angle of the PLF* [21]. From this correlation, a time scale of $2 \sim 3$ zs (1 zs $= 300$ fm/c) of the isospin migration is deduced [23]. It has been found that the neck fragmentation produced in dissipative collisions at Fermi energies carries the isospin information, thus the intermediate mass fragments (IMFs) originating from the neck are influenced by the symmetry energy [24–27]. By inspecting the N/Z composition of the IMFs produced in ternary events in ^{112}Sn + ^{58}Ni at 35 MeV/u, it was found that the IMFs emitted in the early stage are neutron rich and anisotropic in their angular distribution, suggesting the existence of isospin migration and a moderately stiff symmetry energy according to the statistical mean-field calculation [28,29]. Even with these additional probes, it remains crucial to identify more sensitive symmetry-energy probes, particularly observables based on long-time-scale processes.

A good prospective candidate is the fission process of the rotating excited system formed in heavy-ion collisions [30–33]. Since the fission time scale varies from 10^2 fm/c in fast fission to some 10^4 fm/c in fusion fission [34,35] (the specific value depends on the beam energy and the collision centrality), the fission process is sensitive to both long and short timescales. Variation in the emission multiplicities of light charged particles with different N/Z compositions, wherein the scission point is used as a clock, may encode the long-timescale effects of the symmetry energy. A strong (weak) symmetry-energy component will lead to excess neutrons emitted with short (long) timescales.

In this paper, the fission of the excited system formed in Ar + Au at 35 MeV/u is experimentally studied. The fission fragments resulting from decay of the target-like nuclei are measured in coincidence with the light charged particles at various angles in the laboratory. Comparison of the isospin compositions of the light charged particles has been conducted between different angles in the laboratory. A multisource analysis is adopted to describe the energy spectra and reveal the time dependence of the isospin composition of the emitted particles in the fission events. The paper is organized as follows: Section II presents the experimental setup. Section III presents the experimental results. The improved quantum molecular dynamics (ImQMD) model is used to qualitatively interpret the data. Section V is the summary.

II. EXPERIMENTAL SETUP

The experiment was performed in the Large Scattering Chamber at the Heavy Ion Research Facility at Lanzhou (HIRFL). The ^{40}Ar beam with an energy of 35 MeV/u was delivered by the separated sector cyclotron (SSC) and bombarded a self-sustained gold target with a thickness of 674 μg/cm^2. The beam intensity was about 10 nA. The fission fragments were detected by six parallel-plate avalanche counters (PPACs) with an active area of 25×30 cm^2 installed approximately 35 cm from the target. The PPACs adopted the delay-line readout scheme and delivered both the position and the timing signal induced by the fragments. The coincident light charged particles were measured by six silicon telescopes consisting of one (No. 1, 2, 4) or two (No. 3, 5, 6) silicon surface barrier (Au) detectors for energy-loss measurements and a CsI scintillator for residual-energy measurements. The geometric parameters, including the diameter d of the collimator, the distance L to the target, the polar angle θ, the azimuthal angle ϕ, and the thicknesses of the detectors in the six telescopes are listed in Table 1. The energy spectra of the hydrogen isotopes from telescopes 1 and 4 are analyzed and presented in this paper since the isotopic particle identification is achieved in these two telescopes. In order to measure the projectile-like fragments (PLFs), a 12-unit silicon-bismuth-germanate (Si-BGO) hodoscope array organized in two concentric rings was installed 26 cm from the target. The two rings of the telescopes were situated at angles of 9° and 15°, respectively. The thickness of each silicon detector was 150 μm. Figure 1 shows the detector setup.

TABLE I. The parameters of the six LCP telescopes.

	Telescope number					
	1	2	3	4	5	6
d (mm)	12.0	10.2	10.4	14.0	14.0	14.0
L (cm)	11.5	11.5	11.5	26.0	21.6	28.5
θ (°)	158	155	127	80	59	44
ϕ (°)	−90	90	90	−145	−139	−133
ΔE_1 (μm)	50	50	50	50	50	50
ΔE_2 (μm)	400		400	400		
E_{CsI} (mm)	40	40	40	40	40	40

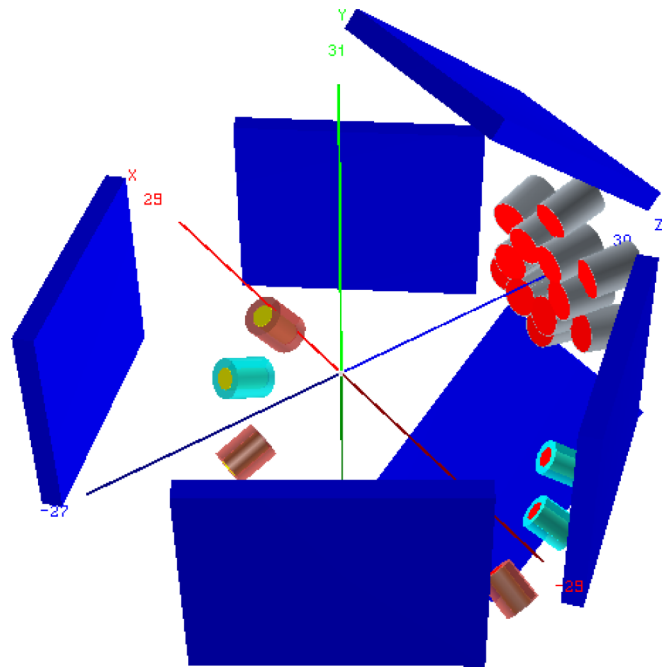

FIG. 1. (Color online) Schematic of detector setup. The beam goes from the lower left to the upper right. The concentric hodoscope is the Si-BGO array. The six large squares are the PPACs, while the six single cylinders represent the LCP telescopes.

The fission events were selected by requiring that two PPACs were fired. The threshold was set higher than the energy-loss signal produced by the LCPs or IMFs, which were hence suppressed. The fission fragments penetrating through the 2-μm-thick mylar foil window triggered the PPACs with very high efficiency. In coincidence with the fission fragments, the main trigger required that at least one particle was detected by the LCP telescopes or the PLF hodoscope. The global starting time signal was provided by the radio frequency of the cyclotron with an uncertainty less than 1 ns. The time walk of the time constant induced by the radio frequency has been corrected by using the alpha particles recorded by the telescopes at a given energy.

III. RESULTS

A. Fission distribution

We first check whether the fission distribution measured in this experiment is consistent with the published literature. For the current system, incomplete fusion cross section is still large according to a recent systematic analysis [36]. The target-like nuclei, or the compound nuclei formed in the incomplete fusion undergo fission processes in competition with evaporation. The fission events can be reconstructed with the conventional folding angle method since the two fission fragments are both detected. The velocity of the fragments are calculated from the flight length and the time of flight deduced from the PPACs. The fission plane, subtended by the two velocity vectors $\mathbf{v}_{f_1}$ and $\mathbf{v}_{f_2}$ of the fission fragments in the laboratory, does not necessarily have to sit on the reaction plane for two reasons: (i) the particle emission modifies the direction of the compound nucleus due to the recoil effect, and (ii) the fission fragments are emitted isotropically in the rest frame of the fissioning nucleus. Assuming $\mathbf{v}_{f_1}$ and $\mathbf{v}_{f_2}$ are the velocities of the fission fragments with masses m_{f_1} and m_{f_2} in the laboratory frame, the reconstructed sum velocity of the compound nucleus $\mathbf{v}_{cn}$ is calculated via momentum conservation:

$$\mathbf{v}_{cn} = \frac{m_{f_1}\mathbf{v}_{f_1} + m_{f_2}\mathbf{v}_{f_2}}{m_{f_1} + m_{f_2}} = \frac{\mathbf{v}_{f_1} + \frac{m_{f_2}}{m_{f_1}}\mathbf{v}_{f_2}}{1 + \frac{m_{f_2}}{m_{f_1}}}. \quad (1)$$

Neglecting the transverse momentum of the target-like nucleus, the mass ratio satisfies

$$\frac{m_{f_2}}{m_{f_1}} = \frac{|\mathbf{v}_{f_1}|_\perp}{|\mathbf{v}_{f_2}|_\perp}, \quad (2)$$

where the subscript $\perp$ represents the projection onto the transverse plane of the reaction. Accordingly, the mass asymmetry η can be obtained via

$$\eta = \frac{1 - \frac{m_{f_2}}{m_{f_1}}}{1 + \frac{m_{f_2}}{m_{f_1}}}. \quad (3)$$

The relative velocity is the difference between the two velocity vectors:

$$\mathbf{v}_{rel} = \mathbf{v}_{f_1} - \mathbf{v}_{f_2}. \quad (4)$$

As a first step, it is of significance to check whether the two fragments exhibit back-to-back alignment that is one of the direct signals characterizing binary decay. Figure 2 presents the azimuthal angle correlation of two fragments. Due to the incomplete geometric acceptance, the range from 220° to 250° for ϕ_1 is not covered. Despite this deficiency, it is shown that the events are all situated along the line $\phi_1 - \phi_2 = 180°$, suggesting the back-to-back feature attributed to a binary decay.

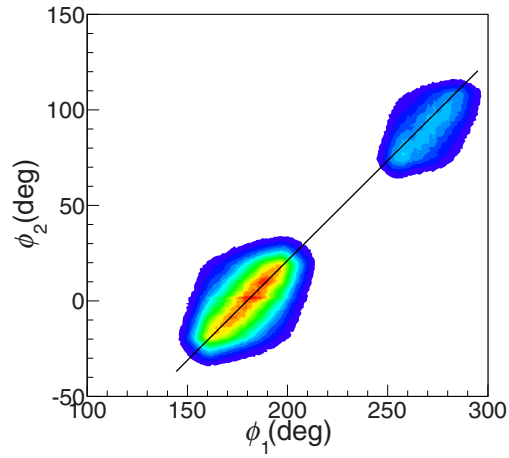

FIG. 2. (Color online) Azimuthal-angle correlation of two fission fragments detected in coincidence.

The fission properties can be further investigated by examining the mass asymmetry and the relative velocity distributions of the two fragments detected in two PPACs. Figures 3(a) and 3(b) present the mass asymmetry and the relative velocity, respectively, as a function of the velocity of the compound nuclei, v_{cn}. The variance of η and the mean value

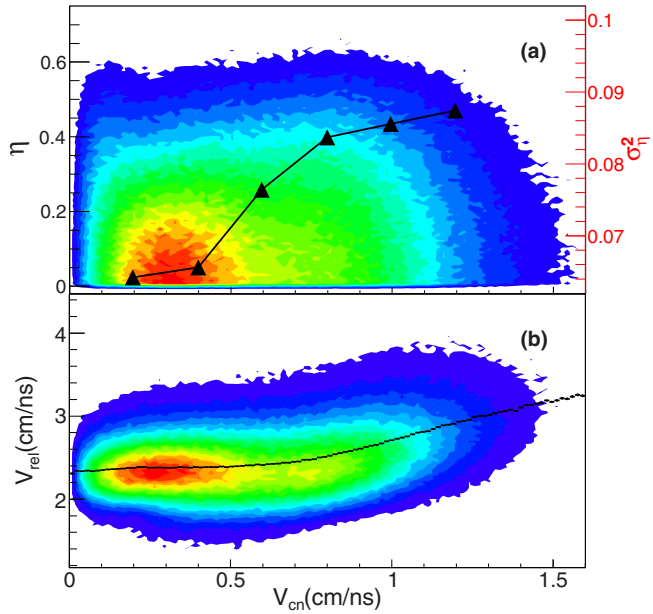

FIG. 3. (Color online) (a) The mass asymmetry and (b) the relative velocity as a function of compound-nucleus velocity. The black solid curves in the two plots represent the variance of η and the mean value of $\mathbf{v}_{rel}$, respectively.

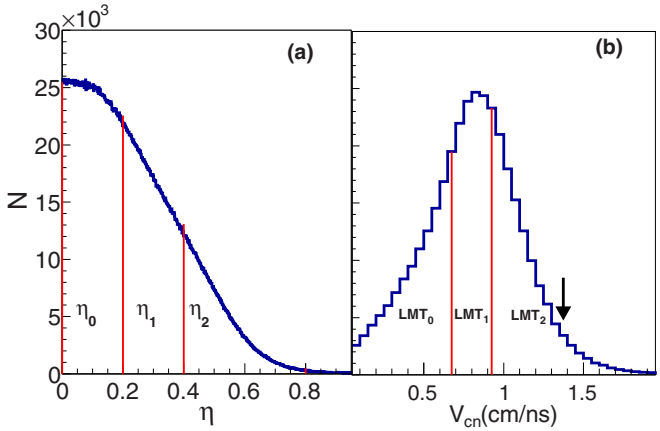

FIG. 4. (Color online) (a) The distribution of the mass asymmetry and (b) the relative velocity of the two fission fragments firing the PPACs. The vertical lines indicate the window cuts used in the moving-source analysis.

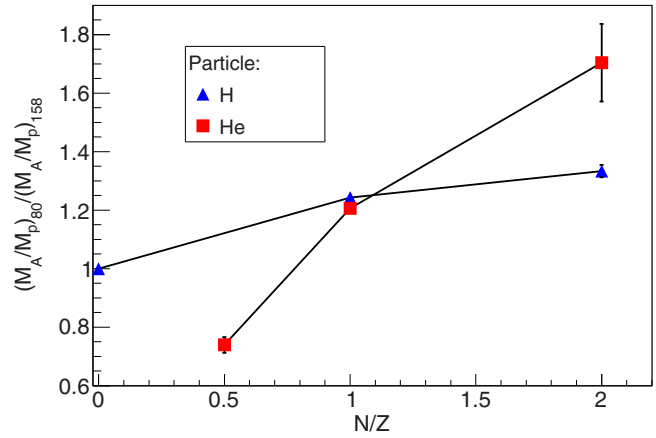

FIG. 5. (Color online) The double yield ratio of LCPs and proton Y_A/Y_p between the telescopes 4 (80°) and 1 (158°) as a function of particle N/Z for hydrogen and helium isotopes.

of $\mathbf{v}_{rel}$ are also presented as solid curves in each plot. Some interesting features are evident. First, in the vicinity of $v_{cn} = 0.28$ cm/ns, the most probable value of the relative velocity appears at about 2.4 cm/ns, in agreement with the Viola systematics for statistical fission. Correspondingly, the mass asymmetry at low v_{cn} peaks at zero indicating a symmetric fission. Second, in the high-v_{cn} range above 0.5 cm/ns, both the mean relative velocity and the variance of the mass asymmetry increase with v_{cn} or the linear momentum transfer (LMT). The increasing trend of σ_η at high LMT is qualitatively consistent with the broadening of the fission-fragment mass distribution as a function of excitation energy observed in reactions using a thorium target induced by various projectiles [37]. Similar results were also reported in Ar + ^{209}Bi at 25 MeV/u, where an increasing trend in both the relative velocity and the mass variance of the fission fragments were observed at high excitation energies [38]. These trends have been explained as evidence of the onset of fast fission (fission without barrier) characterized by a much shorter time scale [39].

Figure 4(a) presents the distributions of the mass asymmetry and Fig. 4(b) presents the compound-nucleus velocity. The vertical lines denote the gates used in the following analysis that uses the moving-source model. The arrow in Fig. 4(b) corresponds to the compound nucleus velocity at full momentum transfer. From the most probable value of $v_{cn} = 0.84$ cm/ns, one derives the linear momentum transfer to be 0.56. This value is consistent with the result in Ar + ^{112,124}Sn system at the same beam energy where the residue was directly identified and the time of flight was recorded [40]. On the other hand, the value of 0.56 is smaller than the empirical estimation of a most probable LMT at 0.72 assuming extreme head-on collisions which, however, overestimates the collision violence (centrality) for the fission events according to the transport-model calculations. The distributions of v_{cn} supports our claim that the events were correctly reconstructed by using the two fission fragments detected in coincidence in the experiment.

B. Analysis of energy spectra

It has been found that the dynamically emitted particles that populate the midrapidity region are more neutron rich than those statistically emitted in events associated with fission of the PLF* [28,41]. In the TLF fission events studied in this work, it is interesting to see if this effect is observed. Regarding the emission source, since the statistical emission source dominates at large angles whereas the dynamical source contributes increasingly to the emission with decreasing angle in the laboratory, it is of interest to compare the N/Z composition of the particles in telescopes 4 (at 80°) and 1 (at 158°). Compared to the telescope at 158°, the telescope at 80° is sensitive to midrapidity emissions, particularly for more energetic particles. Figure 5 shows the double yield ratio of the LCPs and the protons between the two telescopes as a function of N/Z for the hydrogen and helium isotopes. In order to eliminate the solid-angle effect, the yields are normalized to protons in each telescope. With increasing neutron richness, the ratio increases, clearly indicating an enhanced neutron excess in the telescope at $\theta_{lab} = 80°$. The trend shown here is consistent with the observations that the dynamically emitted particles at midrapidity are more neutron rich.

In order to decompose the components from different sources, the moving-source model has been applied to fit the energy spectra and to decompose the contribution from different sources in various LMT and mass asymmetry gates as indicated in Fig. 4. For a given source characterized by the temperature T and Coulomb barrier E_c, the energy spectrum at a given angle θ in the center of mass of the moving source is given by

$$\frac{d^2\sigma}{d\Omega dE} = \frac{N}{2(\pi T)^{3/2}}(E - E_c)^{1/2}\exp[-(E - E_c)/T]. \quad (5)$$

The effect with the laboratory angle θ and the moving source velocity $\mathbf{v}_s$ is included in the Jacobi term $(E_{lab}/E')^{1/2}$ transforming from the center of mass to the laboratory reference frame where E' is

$$E' = E_{lab} + E_s - 2(E_{lab}E_s)^{1/2}\cos\theta, \quad (6)$$

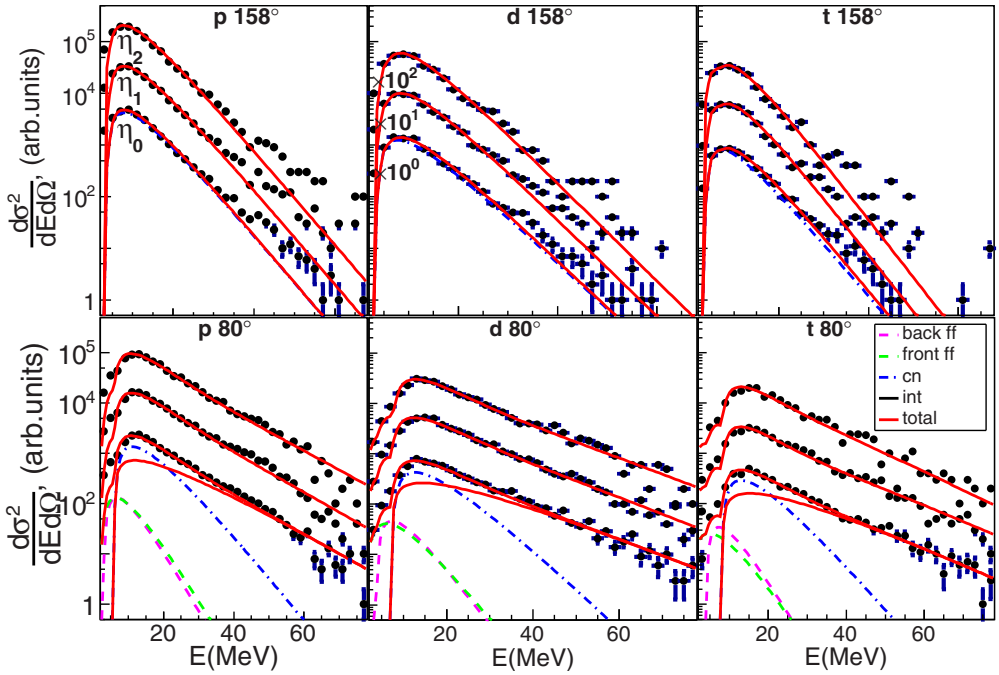

FIG. 6. (Color online) The energy spectra of hydrogen isotopes at 158° (upper panels) and 80° (lower panels) with the moving-source fit in three mass asymmetry windows. For clarity the counts are offset by factors of ten. The total fitting curves are superimposed on all spectra, while the curves of all three moving sources are plotted only for the spectra in the lowest mass asymmetry window, η_0, for a clear display.

with E_s denoting the energy of a particle if moving with the source velocity $\mathbf{v}_s$.

Since the light charged particles are measured in coincidence with the fission fragments, three chronological sources are included in the fitting: (i) the intermediate-velocity source representing the dynamical emissions at early stage (indicated by the subscript "int," (ii) the compound-nucleus source (indicated by the subscript "cn") which represents the statistical emission lasting to the scission point of the TLF* formed in the incomplete fusion, and (iii) the fission-fragment source (indicated by the subscript ff), emitted in both the forward and backward directions. In practice, only the compound-nucleus source is needed to fit the spectra at a large angle of 158°. The single source fitting at large angle helps to reduce the ambiguity in optimizing the fitting parameters. The upper panels in Fig. 6 display the spectra of hydrogen isotopes fit with a single source in the three mass asymmetry gates η_0, η_1, and η_2 defined in Fig. 4. It is shown that the single cn source fitting agrees with the data. The parameters of the cn source obtained at 158° are adopted in the analysis of the energy spectra at 80° by taking into account the geometrical effects. The velocity of the moving source that appeared in Eq. (6) is calculated from the mean sum velocity since the mass asymmetry exhibits an insignificant dependence on v_{cn}, as shown in Fig. 3. The lower panels in Fig. 6 display the spectra fit by three moving sources in three mass asymmetry windows. For the spectra in the lowest mass asymmetry window corresponding to the near symmetrical fission, the curves of each moving source are presented. As mentioned above, the parameters of the cn source are taken from the single-source fitting to the spectra at 158° by taking into account the geometrical acceptance correction. It is shown that the cn source still contributes to the main component of the spectrum while the int source increasingly dominates at the high-energy part approximately above 25 MeV. The emissions from the two fission fragments, with one flying backward and the other flying forward, are located at the low-energy part with a certain separation due to the different kinetics.

In the fitting with three moving sources, the correlation between the fitting parameters exists and special care has been taken since there are nine fitting parameters including the temperature parameter T, Coulomb barrier E_c, and the multiplicity M for each source. Due to the strong correlation between T and E_c, we do not place particular emphasis on the value and the meaning of these two parameters. Instead, only the multiplicities of each source are derived based on a detailed χ^2 analysis. With the parameters of the cn source fixed by the spectra at large angle, the parameters T and E_c for the other two moving sources are varied freely in a wide but physically meaningful range. Then the fitting procedure is used to find the minimum χ^2 for every point on the plane of the two ratios of the three multiplicities, M_{int}/M_{cn} and M_{ff}/M_{cn}. Figure 7 presents the χ^2_{min} contours of the moving source fitting of the spectra of proton (left), deuteron (middle), and triton (right) at 80°. The abscissa denotes M_{int}/M_{cn} while the ordinate denotes M_{ff}/M_{cn}. The three rows represent the three windows on the mass asymmetry η of the two correlated fission fragments. The solid stars are plotted at the positions where the lowest χ^2_{min} are located.

The locations of the minimum χ^2 are summarized in Fig. 8 and reveal the average N/Z composition of the LCPs emitted from different sources. Figure 8(a) presents the ratio of the emission multiplicity of the intermediate-velocity source over the one of the compound-nucleus source for the hydrogen

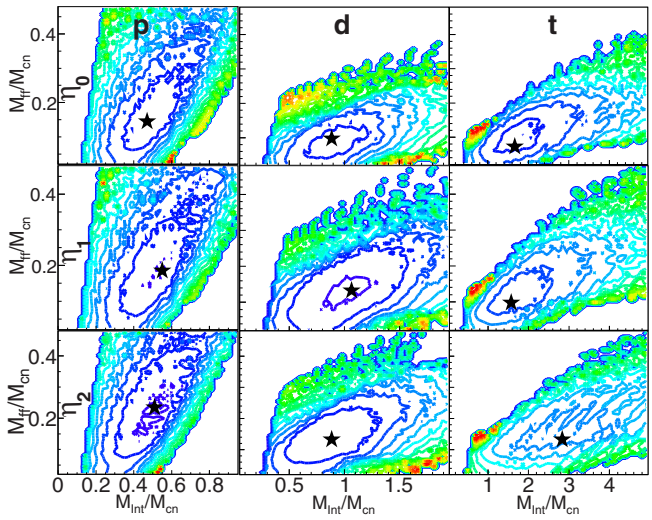

FIG. 7. (Color online) The χ^2_{min} distribution of the moving-source fits to the spectra of hydrogen isotopes in three mass asymmetry gates. Each value on the contour is obtained by searching the minimum χ^2 in a wide space of T and E_c while keeping the two multiplicity ratios fixed. The solid stars indicate the lowest χ^2_{min} locations.

isotopes at different mass asymmetry. The error bars represent the uncertainty corresponding to an increase of the χ^2 by 20% from each respective lowest amplitude. It is shown that, despite the large error bars, the ratio increases from proton (squares) to triton (inverted triangles), indicating that more neutrons bounded in the hydrogen isotopes are emitted with the intermediate velocity source, which corresponds to an earlier-stage emission compared to the statistical emission. The hierarchy from proton to triton are evident and exhibits insignificant dependence on the mass asymmetry, except for the case of triton, for which the large error bars hinder further quantitative conclusions. The hierarchy of the M_{int}/M_{cn} ratio from proton to deuteron and triton agrees quantitatively with the previous model independent comparison in Fig. 5. Moreover, with the postulation that the early dynamic emission originates from the neck formed between the projectile-like and the target-like nuclei [27], the hierarchy of the M_{int}/M_{cn} ratio also suggests a neutron-rich neck in agreement with the previous predictions and observations [24,27].

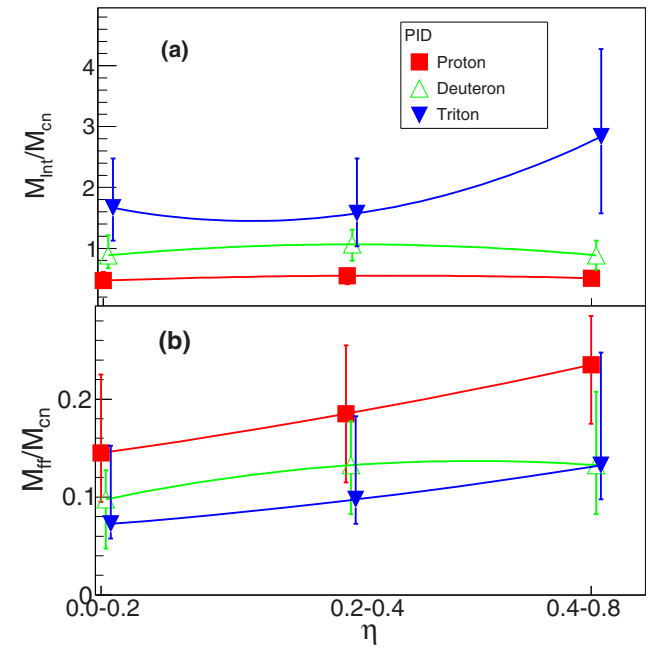

FIG. 8. (Color online) The upper panel shows the multiplicity from the intermediate velocity (int) source and the lower panel shows that from the fission fragment (ff) source, both normalized to the multiplicity from the compound -nucleus (cn) source.

Figure 8(b) presents the multiplicity summed over the two fission-fragment sources similarly normalized to the compound-nucleus source as a function of the mass asymmetry η. An inverse trend is visible that the yield ratio decreases from proton to triton, despite the large error bars. Since the fission fragment source represents the postscission emission, the inverse trend indicates a decreasing neutron richness of the particles emitted along the long decay chain of the TLF. Moreover, the ratio M_{ff}/M_{cn} shows an slightly positive slope along the mass asymmetry. This trend is consistent with the fact that, as the mass asymmetry becomes larger, the system reaches the scission point more quickly, resulting in a relatively higher postscission multiplicity. The same trend was reported in Xe + Ti reactions at 18.5 MeV/u [39]. This result is also consistent with the inference of Fig. 3 that a larger mass asymmetry variance corresponds to a short fission time scale. Nevertheless, we note here that the large errors for the fission fragments can be reduced if a lower detection threshold is achieved and more telescopes at different polar angles can be simultaneously included for fitting.

The multiplicity ratios in different v_{cn} or linear momentum transfer (LMT) gates reveal the same information. Figure 9 shows the energy spectra of proton, deuteron, and triton at $\theta_{lab} = 158^\circ$ (upper) and $\theta_{lab} = 80^\circ$ (lower) at three LMTs derived from the target-like fragment velocity as shown in Fig. 4. As in the case of Fig. 6, the spectra were fit using three moving sources, cn, int, and ff at $\theta_{lab} = 80^\circ$. The parameters of the cn source are obtained by a single-source fit to the energy spectra at $\theta_{lab} = 158^\circ$. Unlike the fitting in Fig. 6, however, in this case the cn source velocity is computed in each v_{cn} gate. Figure 10 displays the ratios M_{int}/M_{cn} (upper) and M_{ff}/M_{cn} (lower) as a function of v_{cn}. It is also shown that, for all the LMT gates, the ratio M_{int}/M_{cn} increases from proton to deuteron and triton. In contrast, the ratio M_{ff}/M_{cn} for protons is larger than that of deuterons and tritons, although the difference between the latter two is again not easily discernible due to the large error bars. The different behavior between M_{int}/M_{cn} and M_{ff}/M_{cn} suggests that the neutron excess of the dynamically emitted light charged particles is relatively high and the neutron richness decreases along the long decay chain.

C. Improved quantum molecular dynamics analysis

In order to view the time-dependent isospin composition of the emission particles in the fission process, an improved quantum molecular dynamics (ImQMD) model is utilized to simulate the fission process of $^{40}Ar + ^{197}Au$ at 35 MeV/u. In the ImQMD model [42,43], as in the original QMD model [44],

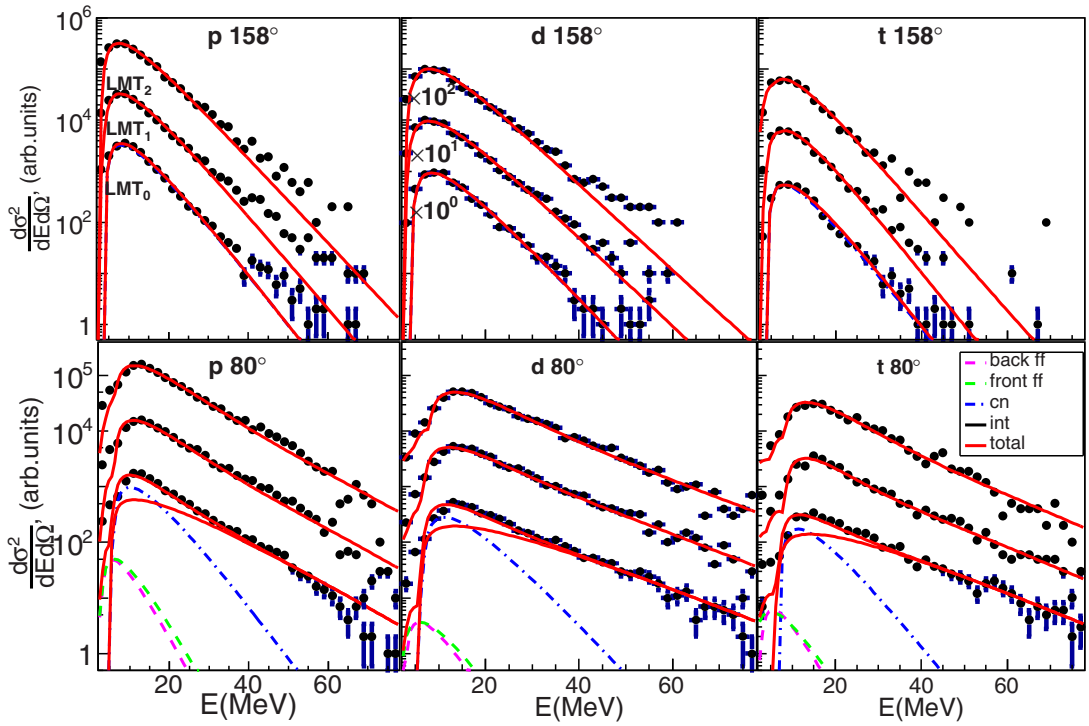

FIG. 9. (Color online) The energy spectra with the moving source fitting for hydrogen isotopes in three LMT gates. For clarity the counts with LMT1 and LMT2 are offset by 10 and 100, respectively. The legends are the same as those in Fig. 6.

each nucleon is represented by a coherent state of a Gaussian wave packet. The density distribution function ρ of a system reads

$$\rho(\mathbf{r}) = \sum_i \frac{1}{(2\pi\sigma_r)^{3/2}} \exp\left[-\frac{(\mathbf{r}-\mathbf{r}_i)^2}{2\sigma_r^2}\right], \tag{7}$$

where σ_r denotes the width of the wave packet for nucleons in coordinate space and the subscribe i denotes the i^{th} nucleon.

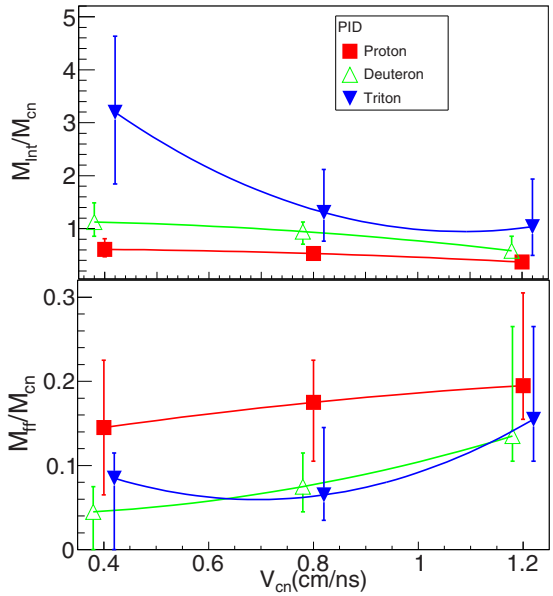

FIG. 10. (Color online) Same as Fig. 8; the ordinate is the velocity of the compound nucleus reconstructed from the two fragments.

The nuclear interaction potential energy U_{loc} is obtained from the integration of the Skyrme energy density functional $V_{\text{loc}}[\rho(\mathbf{r})]$,

$$V_{\text{loc}} = \frac{\alpha}{2}\frac{\rho^2}{\rho_0} + \frac{\beta}{\sigma+1}\frac{\rho^{\sigma+1}}{\rho_0^{\sigma}} + \frac{g_0}{2\rho_0}(\nabla\rho)^2 + \frac{C_s}{2}\left[\frac{\rho^{\gamma+1}}{\rho_0^{\gamma}} - \frac{\kappa_s}{\rho_0}(\nabla\rho)^2\right]\delta^2 + g_\tau\frac{\rho^{\eta+1}}{\rho_0^{\eta}}, \tag{8}$$

where $\delta = (\rho_n - \rho_p)/(\rho_n + \rho_p)$ is the isospin asymmetry. The first three terms in the above expression can be obtained directly from the potential-energy functional of Skyrme forces. The last term ($\rho\tau$ term) is obtained by using the Thomas–Fermi approximation for the kinetic-energy-density functional. The fourth term is the symmetry-energy potential part where both the bulk- and the surface-symmetry energy are included. Here, C_s is the symmetry potential strength parameter, and γ describes the density dependence of symmetry energy. Thus by varying γ in the ImQMD model, one can mimic different density dependence of the symmetry energy. For instance, $\gamma = 1$ denotes a stiff symmetry energy with nearly linear density dependence, while $\gamma = 2$ and 0.5 correspond to an extra-stiff and a soft symmetry energy, respectively. To describe the fermionic nature of the N-body system and to improve the stability of an individual nucleus, the phase-space occupation constraint method [45] and the system-size-dependent wave-packet width $\sigma_r = 0.94 + 0.018A^{1/3}$ are adopted. In this work, we adopt the parameter set IQ3 [46,47], which has been applied in the study of multifragmentation at intermediate energies and heavy-ion fusion reactions at incident energies around the Coulomb barriers. The parameter values are listed in Table II.

TABLE II. The IQ3 parameter set used in ImQMD simulations [46,47].

α	207 MeV	β	138 MeV
σ	7/6	g_0	18 MeV fm^2
C_s	32 MeV	κ_s	0.08 fm^2
g_τ	14 MeV	η	5/3

Figure 11 presents the average neutron-to-proton ratio $\langle N/Z\rangle$ of the light particles as a function of time in the ImQMD simulation. The distance between the projectile and the target nuclei is 30 fm at $t = 0$. The contact time of their surfaces occurs at about 110 fm/c, as indicated by the vertical arrows. Since the transport-model recognizes clusters by using a coalescence algorithm and normally overestimates the yield of nucleons but underestimates that of clusters depending on the coalescence parameter, all the particles with $Z \leqslant 3$ are summed in the calculations of the average $\langle N/Z\rangle$ of the emitted products. The left panel presents the average $\langle N/Z\rangle$ for the inclusive collisions while the right panel presents that for the fission events. To see the effect of the stiffness of the symmetry energy, two gamma values, $\gamma = 0.5$ and 2, have been adopted in the simulation, respectively. Some interesting features are visible. First, along the whole decay chain, the average $\langle N/Z\rangle$ decreases with time. Particularly, at very early stages of the collision and subsequent decay; namely, prior to 250 fm/c, the average ratio $\langle N/Z\rangle$ is largely enhanced compared to the values at late stage and the relative enhancement exhibits a dependence on the symmetry energy. There are two possible reasons for the enhancement of N/Z in the early stages. One is the contact of the neutron skin at the early stage, the other is the fast emission of the nucleons. It is consistent with the picture that the neutron richness of the emitted particles is enhanced at the beginning stage of the emission in qualitative agreement with the experimental hierarchy of the ratio $M_{\rm int}/M_{\rm cn}$. Second, the isospin composition $\langle N/Z\rangle$ exhibits an obvious dependence on the stiffness of the symmetry energy. With a soft parameter $\gamma = 0.5$, the value of the symmetry energy below saturation density is large. Hence the effect of the neutron-to-proton asymmetry is strong

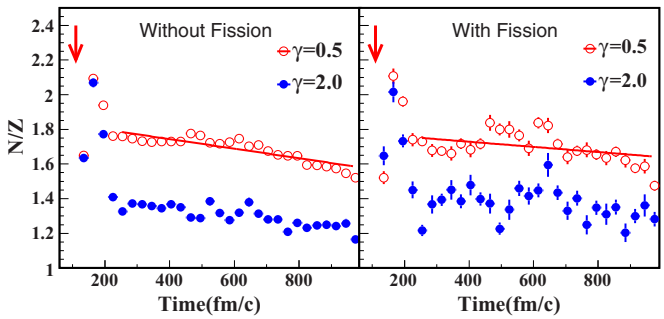

FIG. 11. (Color online) The average $\langle N/Z\rangle$ summed for the light particles with $Z \leqslant 3$ as a function of time with $\gamma = 0.5$ (soft, open circles) and $\gamma = 2$ (stiff, solid circles) in ImQMD simulation for (left panel) the inclusive events and (right panel) the selected fission events. The vertical arrows show the contact time of the projectile and the target.

and the isospin fractionation mechanism moves more neutrons into the gas phase. Consequently, the light particles exhibit an enhanced $\langle N/Z\rangle$ over the system value of 1.44. In the case of a stiff value for the symmetry-energy parameter, $\gamma = 2$, the degree of isospin fractionation is weak and the $\langle N/Z\rangle$ of the light particles is comparable with the system value of 1.44. The relative difference between the two symmetry energy parametrizations is about 20% along the whole process up to 1000 fm/c, which indicates that the isospin composition of the emitted particles is an effective probe to the symmetry energy. The long-time effect of the symmetry energy is consistent with the experimental demonstration in Ref. [23] that the effect of isospin drift or diffusion in a dinuclear system exists with a timescale up to 1200 fm/c. By comparing the left and right panels, one finds that the effect of the symmetry energy remains equally significant in the fission events even though the fission condition may set a selection to the collision geometry. It suggests that the scission point can be used experimentally as a clock to probe the effect of the symmetry energy in the processes with long time scale. We note that, to arrive at a quantitative reproduction of the data, transport-model calculations with careful treatments of the clustering and of the cascade decay of all excited fragments are required. Meanwhile, further experiments using the detector with improved geometric coverage, or even better with 4π coverage, are preferred to reduce some of the uncertainties associated with the analysis.

IV. SUMMARY

In summary, the fission fragments in the reaction ^{40}Ar + ^{197}Au at 35 MeV/u are measured in coincidence with the light charged particles. By using the folding-angle method, the fission events are reconstructed. By comparing the relative yield of the light charged particles detected at $\theta_{\rm lab} = 80^\circ$ and 158°, it is found that the particles emitted at smaller angles with a larger contribution from the earlier stages of emission are more neutron rich compared with the compound-nucleus emissions which dominate the emissions at larger angles. By using the multiple-moving-source fitting technique, the contribution to the kinetic-energy spectra of light charged particles from three sources, i.e., the intermediate-velocity source, the compound-nucleus source, and the fission-fragment source, are decomposed. A hierarchy of the multiplicity ratio between the intermediate-velocity source and the compound-nucleus source has been observed. The ratio $M_{\rm int}/M_{\rm cn}$ increases systematically for $Z = 1$ particles as A increases. This trend occurs for all mass asymmetries of the fission events. It confirms the picture that the particles emitted at earlier stage are more neutron rich. An inverse trend is observed in the particle multiplicities from the fission-fragment source. This finding is consistent with the previous results observed in the fission of excited PLF [23]. It is further demonstrated by the ImQMD model calculation that the neutron excess of the light particles is larger for the early emission and decreases monotonically with time. It is noteworthy that this systematic decrease in N/Z persists for times as long as 1000 fm/c. Within the model calculations, the time dependence of the N/Z composition of the emitted LCPs exhibits a dependence on the value of the symmetry energy parameter at subsaturation density.

ACKNOWLEDGMENTS

This work was supported by the Natural Science Foundation of China under Grants No. 11375094 and No. 11079025, and by Tsinghua University Initiative Scientific Research Program. The authors thank Professor B. Tsang from Michigan State University and Professor M. Bisset from Tsinghua University for the careful reading of the manuscript and valuable discussions.

[1] B. A. Li, L. W. Chen, and C. M. Ko, Phys. Rep. **464**, 113 (2008).
[2] M. B. Tsang *et al.*, Phys. Rev. C **86**, 015803 (2012).
[3] L. G. Sobotka, Phys. Rev. C **50**, R1272 (1994).
[4] H. S. Xu *et al.*, Phys. Rev. Lett. **85**, 716 (2000).
[5] M. B. Tsang *et al.*, Phys. Rev. Lett. **92**, 062701 (2004).
[6] B. A. Li *et al.*, Nucl. Phys. A **735**, 563 (2004).
[7] L.-W. Chen, C. M. Ko, and B.-A. Li, Phys. Rev. Lett. **94**, 032701 (2005).
[8] H. Y. Wu *et al.*, Phys. Lett. B **538**, 39 (2002).
[9] B.-A. Li, C. M. Ko, and Z. Ren, Phys. Rev. Lett. **78**, 1644 (1997).
[10] M. A. Famiano *et al.*, Phys. Rev. Lett. **97**, 052701 (2006).
[11] M. B. Tsang, W. A. Friedman, C. K. Gelbke, W. G. Lynch, G. Verde, and H. S. Xu, Phys. Rev. Lett. **86**, 5023 (2001).
[12] L.-W. Chen, C. M. Ko, B.-A. Li, and J. Xu, Phys. Rev. C **82**, 024321 (2010).
[13] T. Li, U. Garg *et al.*, Phys. Rev. C **81**, 034309 (2010).
[14] M. B. Tsang, Y. Zhang, P. Danielewicz, M. Famiano, Z. Li, W. G. Lynch, and A. W. Steiner, Phys. Rev. Lett. **102**, 122701 (2009).
[15] Y. G. Ma *et al.*, Phys. Rev. C **85**, 024618 (2012).
[16] Y. B. Wei, Y. G. Ma *et al.*, Phys. Lett. B **586**, 225 (2004).
[17] Y. G. Ma, Y. B. Wei *et al.*, Phys. Rev. C **73**, 014604 (2006).
[18] L.-W. Chen, V. Greco, C. M. Ko, and B.-A. Li, Phys. Rev. Lett. **90**, 162701 (2003).
[19] Z. G. Xiao, R. J. Hu *et al.*, Phys. Lett. B **639**, 436 (2006).
[20] M. Liu, N. Wang, Z.-X. Li, and F.-S. Zhang, Phys. Rev. C **82**, 064306 (2010).
[21] S. Hudan *et al.*, Phys. Rev. C **86**, 021603(R) (2012).
[22] C. Rizzo, V. Baran, M. Colonna, A. Corsi, and M. Di Toro, Phys. Rev. C **83**, 014604 (2011).
[23] K. Brown *et al.*, Phys. Rev. C **87**, 061601(R) (2013).
[24] N. Wang, X. Wu, and Z. Li, Phys. Rev. C **67**, 024604 (2003).
[25] V. Baran, M. Colonna, and M. Di Toro, Nucl. Phys. A **730**, 329 (2004).
[26] M. Di Toro, *Contribution to the 5th Italy-Japan Symposium, Recent Achievements and Perspectives in Nuclear Physics, Naples Nov. 3–7, 2004* (World Scientific, Singapore, 2005).
[27] S. Piantelli *et al.*, Phys. Rev. Lett. **88**, 052701 (2002).
[28] E. De. Filippo *et al.*, Phys. Rev. C **86**, 014610 (2012).
[29] E. De. Filippo, J. Phys.: Conf. Ser. **420**, 012105 (2013).
[30] D. J. Hinde *et al.*, Phys. Rev. C **39**, 2268 (1989).
[31] D. J. Hinde, R. du Rietz, M. Dasgupta, R. G. Thomas, and L. R. Gasques, Phys. Rev. Lett. **101**, 092701 (2008).
[32] Z. Y. He *et al.*, Chin. Phys. Lett. **15**, 13 (1998).
[33] M. B. Tsang *et al.*, Phys. Rev. C **44**, 2065 (1991).
[34] G. Casini *et al.*, Phys. Rev. Lett. **71**, 2567 (1993).
[35] J. W. Zheng *et al.*, High Energy Phys. Nucl. Phys. **23**, 946 (1999) (in Chinese).
[36] P. Eudes, Z. Basrak *et al.*, Europhys. Lett. **104**, 22001 (2013).
[37] S. Harar, Nucl. Phys. A **471**, 205 (1987).
[38] J. W. Zheng *et al.*, High Energy Phys. Nucl. Phys. **23**, 409 (1999) (in Chinese).
[39] M. Gui *et al.*, Phys. Rev. C **48**, 1791 (1993).
[40] Z. G. Xiao *et al.*, High Energy Phys. Nucl. Phys. **25**, 643 (2001) (in Chinese).
[41] Z. Kohley *et al.*, Phys. Rev. C **86**, 044605 (2012).
[42] N. Wang, Z. X. Li, and X. Z. Wu, Phys. Rev. C **65**, 064608 (2002).
[43] N. Wang, Z. Li, X. Wu, J. Tian, Y. X. Zhang, and M. Liu, Phys. Rev. C **69**, 034608 (2004).
[44] J. Aichelin, Phys. Rep. **202**, 233 (1991).
[45] M. Papa, T. Maruyama, and A. Bonasera, Phys. Rev. C **64**, 024612 (2001).
[46] V. Zanganeh, N. Wang, and O. N. Ghodsi, Phys. Rev. C **85**, 034601 (2012).
[47] C. Li, J. L. Tian, L. Ou, and N. Wang, Phys. Rev. C **87**, 064615 (2013).